ECS Transactions, 78 (1) 667-675 (2017)
10.1149/07801.0667ecst ©The Electrochemical Society

Electrochemical Behavior of Nanostructured $La_{0.8}Sr_{0.2}MnO_3$ as Cathodes for Solid Oxide Fuel Cells

Joaquín Sacanell[a,b], J. Hernández Sánchez[a], A. E. Rubio Lopez [a], H. Martinelli [a], J. Siepe [a] A. G. Leyva [a,c], V. P. Ferrari [a,b], M. Pruneda[d], D. Juan [a,b], and D. G. Lamas [a,b,c]

[a]Departamento de Física de la Materia Condensada, Gerencia de Investigación y Aplicaciones, Centro Atómico Constituyentes, Comisión Nacional de Energía Atómica, Av. General Paz 1499 (1650) Buenos Aires, Argentina
[b] CONICET, Argentina
[c] Escuela de Ciencia y Tecnología, Universidad Nacional de General San Martín Martín de Irigoyen 3100, Edificio Tornavía, Campus Miguelete (1650) San Martín, Pcia. de Buenos Aires, Argentina
[d] Catalan Institute of Nanoscience and Nanotechnology (ICN2), CSIC and The Barcelona Institute of Science and Technology, Campus Bellaterra, 08193 Barcelona, Spain

$La_{0.8}Sr_{0.2}MnO_3$ (LSM) is one of the most commonly used cathodes in Solid Oxide Fuel Cells (SOFC). In spite of the fact that nanostructured cathodes are expected to display improved performance, the high operating temperature (~ 1000°C) of LSM-based SOFCs hinders their stability. In the present work, we have developed nanostructured cathodes prepared from LSM nanotubes of enhanced performance, allowing its use at lower temperatures (~ 800°C). We observed that our cathodes have qualitative improvements compared with microstructured materials: firstly, the diffusion in the gas phase is optimized to a negligible level and secondly, evidence of ionic conduction is found, which is extremely rare in LSM cathodes. We propose that this important change in the electrochemical properties is due to the nanostructuration of the cathode and deserves further attention, including the exploration of other materials.

Introduction

A large amount of work has been devoted in the last years to the study of novel materials and structures to enhance the properties of Solid Oxide Fuel Cell (SOFC) (1) components, i.e. the electrodes (2-14) and the electrolyte (15-18). The cathode is usually an electronic conductor with the capability of catalyzing the oxygen reduction reaction (ORR), but in this case the ORR can only take place in the triple phase boundary (TPB) between gas, electrolyte and electrode. Thus, the electrode must be highly porous. The $La_{0.8}Sr_{0.2}MnO_3$ manganite (LSM) is the most widely used cathode for SOFCs (19-25). Several works have been devoted to improve its performance by increasing the number of active sites for the ORR. The main limitation is the poor ionic conductivity, which can be increased by mixing LSM and Yttria Stabilized Zirconia (YSZ). This limitation could be overcome by the use of mixed electronic and ionic conductors (MIEC), in which the ORR can occur throughout the whole surface of the cathode. However, long term studies have shown that most known MIEC materials are unstable under operating conditions.

The electrochemical activity of the cathode strongly depends on its microstructure, as shown for nanostructured MIEC materials,(3-14) and porosity, as have been demonstrated for LSM (22-25) as well as several MIECs which can be used as intermediate temperature SOFC (IT-SOFC) cathodes (6,7,9,10). In this last case, one successfully explored possibility was the use of submicrometric tubes or rods, that have shown to improve both gas access and ionic conductivity (9,10).

In the case of manganites, the use of nanostructure (26) was initially discarded due to the high temperatures needed for the oxygen reduction to occur. However, if a significant improvement is obtained, their use as an IT-SOFC cathode would be possible. Nevertheless, the intrinsic limitation of the ORR in the TPB remains being their most important drawback.

Oxygen tracer diffusion experiments have shown that grain boundary diffusion is faster than through bulk and therefore, microstructure could in principle enhance the performance of LSM cathodes (27,28).

Due to poor ionic conductivity, the performance of LSM based cathodes is generally limited by the charge transfer process (29-33), while the behavior of MIECs is determined by their significant oxygen ion conduction (34).

In this work, we present a study of the electrochemical behavior of a SOFC cathode prepared from LSM nanotubes.The resulting nanostructure was a collection of dense rods formed by agglomerated nanoparticles. Our results show an enhancement of the electrochemical properties, with reminiscences of systems with significant oxygen diffusion, such as composite LSM-YSZ and also MIEC conductors cathodes. We also show an improvement of the access of oxygen resulting in a negligible contribution of gas phase transport to the resistance.

Materials and Methods

LSM nanotubes preparation is described elsewhere (35). The YSZ electrolyte substrates were prepared by pressing pellets of commercial ZrO_2-8%Y_2O_3 powder (Tosoh) into 10 mm diameter discs of about 1 mm thickness, which were then fired at 1600ºC for 4 hrs.

We performed cathode deposition by painting both sides of the electrolytes with an ink prepared with LSM nanotubes and a commercial ink vehicle (IV, NexTech Materials^{TM}), to make symmetrical cells. It was dried with an infrared lamp, and fired at different temperatures between 950 and 1200ºC. The resulting electrode is a collection of dense rods. Even after performing the thermal treatment to attach the cathode the surface remains highly porous (9,10). In the following, we present a study of cathodes fired at 1000°C using nanotubes of 400 nm of diameter.

Electrochemical Impedance Spectroscopy (EIS) measurements were performed as a function of T and the oxygen partial pressure ($p(O_2)$). Polarization Resistance (RP) values were determined from EIS data as the difference between the low frequency and the high frequency intercepts with the real axis in the Nyquist plot. Additional experimental details can be found in previous works (9,10).

Results and Discussion

Nyquist plots measured in air are shown in Figure 1. We see a very small contribution at small frequencies even at low T, and a single impedance arc is observed in the whole temperature range. Pure LSM cathodes usually show a dominant low frequency arc (29,30), which can be reduced by mixing LSM with YSZ, i.e. with an ionic conductor. In contrast, the arc shown in Figure 1 has similar features to those observed for composite LSM/YSZ cathodes (36) or MIEC materials, dominated by adsorption and fast oxide-ion diffusion (34). The slight asymmetry observed at larger frequencies, signal of a Warburg element, is another reminiscence of MIEC cathodes (10,12).

We can see that the imaginary part drops very fast for f > 1000 Hz, and it is negligible for f < 10 Hz. The RP values, lower than 1 Ωcm2 for temperatures above 750ºC, are close to those reported for microstructured LSM-YSZ composites (19,20,23,24). In Figure 2, we show the dependence of ($T\ R_P^{-1}$) vs. 1000/T. We can assume the following Arrhenius relation:

$$T/R = 1/R_{P0} \exp\left(-E_a/k_B T\right) \qquad [1]$$

where R_{p0}^{-1} is a constant pre-exponential factor, T is the absolute temperature, k_B is the Boltzmann constant and E_a is the activation energy of the overall process.

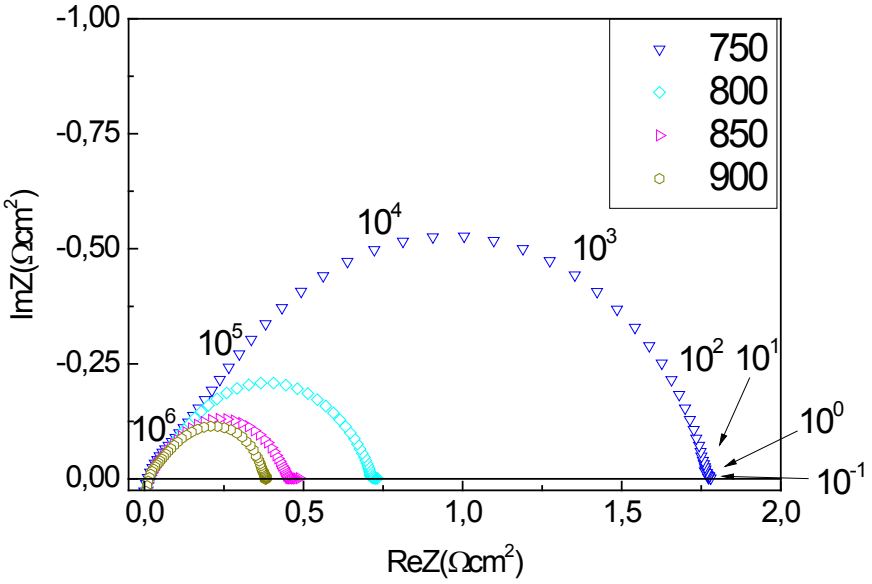

Figure 1. Nyquist plots for the nanostructured LSM cathode for the 750 – 900ºC range. The numbers close to the measured data at 750ºC indicate the measurement frequency in Hz.

A value of E_a = 1.52 eV is obtained for T < 800ºC, lower than the typical activation energies observed for pure LSM,(31,37) and close to that obtained in LSM/YSZ composite cathodes.(29,38,39) For T > 800ºC, E_a = 0.86 eV, reduced to almost half of the low T value. Therefore, the cathode exhibits two different operating regimes.

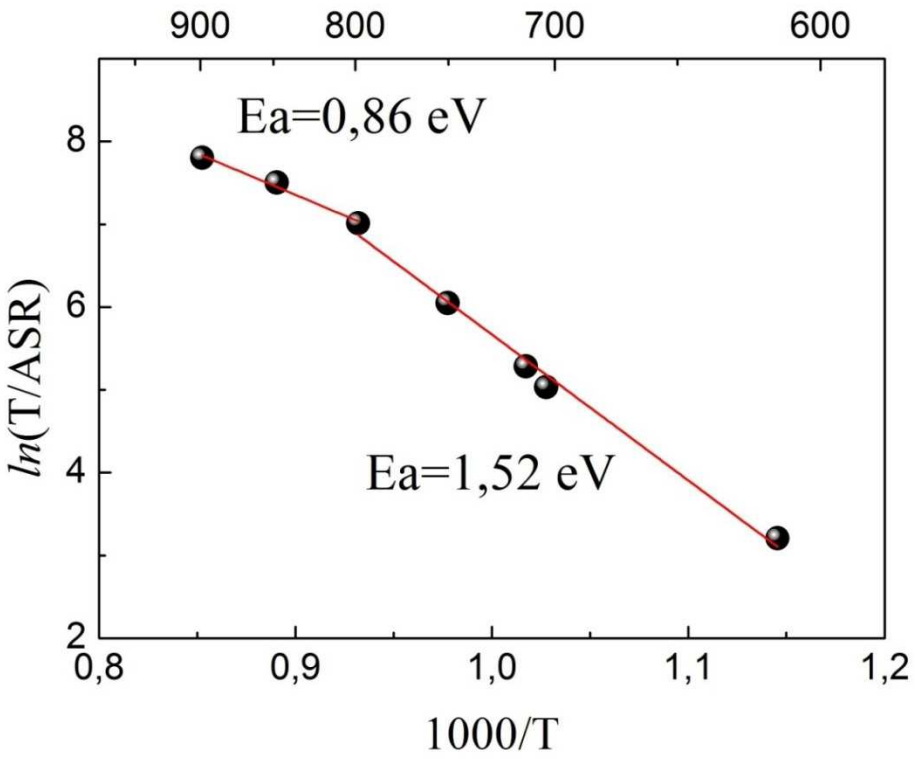

Figure 2. Arrhenius plot of T/R_P and activation energies above and below 800ºC.

The typical low frequency (f < 10 Hz) contribution of LSM cathodes (see (19,34,40,41,42,43) and references therein) is not present in our measurements, generally attributed to gas phase transport.(34) So, the nanostructure seems to optimize the gas access to the surface making its contribution negligible. To confirm the above hypothesis, we performed EIS measurements at reduced O_2 partial pressures ($p(O_2)$), shown in Figure 3(a).

We observe that the reduction of the oxygen partial pressure induces the relative growth of the aforementioned process, evidenced as an additional arc at low frequencies. The use of our nanostructure gives rise to this overwhelming effect, evidently related with the increase of active sites for the ORR.

In order to separate the several contributions to the impedance according to their characteristic time, it is useful to consider them as arising from parallel RQ equivalent circuits in series (44), each of them with a resistance (R) and a pseudocapacity or constant phase element (Q). A model with three (RQ) components was tested initially but, as the (RQ) component corresponding to intermediate frequencies has an exponent consistent with a finite length Warburg element[*], the EIS data were fitted using a $(R_1Q_1)W(R_2Q_2)$ equivalent circuit. The two parallel RQ components are both in series, and in series with a finite length Warburg element. The R_1Q_1 element was added to account for a process at high frequencies which is not evident but needed to adequately fit the data.

[*] The impedance of a constant phase element is $[(j\omega)\alpha Y_0]$-1, where Y_0 is constant. If $\alpha = 0$ the element is a resistance, if $\alpha = 1$ the element is a capacitor, while if $\alpha = 0.5$ it corresponds to a Warburg element. In our case, $\alpha = 0.46 \pm 0.07$.

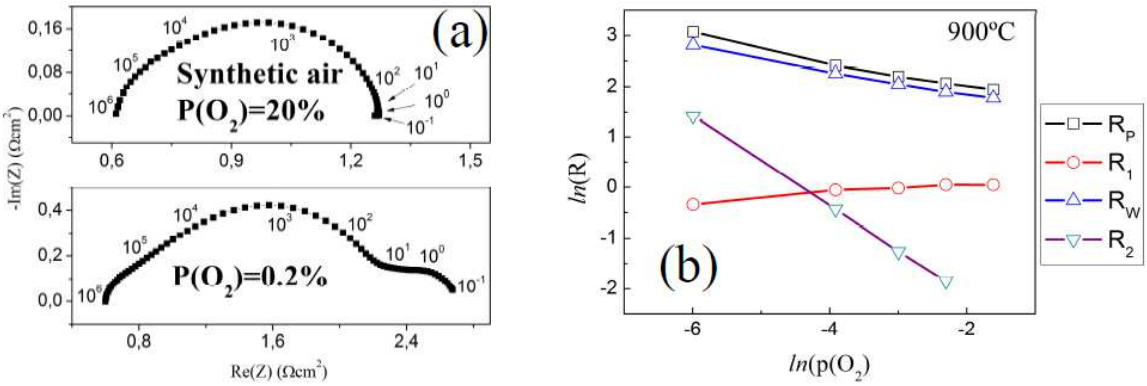

Figure 3. (a) Nyquist plots for different oxygen partial pressures; (b) Oxygen partial pressure dependence of the resistive part of each of the components of the impedance. (square) overall RP, (circle) high frequency RQ, (up triangle) Warburg element, (down triangle) low frequency RQ.

In Figure 3(b), we show the dependence of the resistive part of each process as a function of oxygen partial pressure. It can be noticed that the overall R_P is clearly dominated by the intermediate frequency process.

The high frequency part of the spectra (from 1 MHz to 100 kHz), modelled by (R_1Q_1), is generally attributed to ionic transfer process between the cathode and the electrolyte,(29,32,45) which is independent of the surrounding gas atmosphere. The intermediate frequency region (below 10 kHz), which is the dominant contribution, is more adequately described by the finite length Warburg element, as is usually observed in La-Sr cobaltites.(10,12,34) For the low frequency process that is hindered at atmospheric pressure we added an extra (R_2Q_2) term centred around ~ 1-10 Hz.

The resistivity of each of the components was fitted using the classical power law dependence:

$$R_i \propto P(O_2)^{-n} \qquad [2]$$

The subscript "*i*" stands for each process, while the value of "*n*" gives information about the type of species involved in the reaction that gives rise to this component (43).

The total polarization resistance can be well fitted with $n = 0.25 \pm 0.02$. This value is a signature of the redox reaction between the adsorbed oxygen and the bulk electrode material (45,46):

$$O_{ad} + V_O^{\cdot\cdot} + 2\,e' = O_O \qquad [3]$$

where O_{ad} is an oxygen atom adsorbed on the surface of the cathode, $V_O^{\cdot\cdot}$ is a double positively charged oxygen vacancy, *e*' is an electron and O_O is an oxygen ion in the oxygen site. This is the process usually referred to as "charge transfer" and is dominant in MIECs as LSC or LSCF (31) and in LSM-YSZ composites.(29,30,33) The common feature of the references of the literature reporting similar electrochemical properties is that they refer to cathodes in which a significant ionic conductivity is expected, in contrast to what is expected in pure LSM.

The low-frequency component becomes visible as $p(O_2)$ drops. We can observe that it shows the most important change with $p(O_2)$. As shown in Figure 4, this component is significant for frequencies below 10 Hz, a region usually dominant in LSM cathodes. Moreover, the fitting analysis with Equation (2) gives a value of $n = 0.89 \pm 0.01$. This value is close to 1, which corresponds to gas phase diffusion as a limiting step (29,30,32,40,45,47).

Our results thus confirm that the nanostructure produces a qualitative change of the cathodic properties even in the case of a poor ionic conductor such as LSM.

The overall observed results depict a novel behaviour that can be summarized as follows: At high temperature (T > 800°C), the $p(O_2)$ dependence is consistent with a dominant charge transfer process, with an $E_a = 0.86$ eV. At low temperature, $E_a = 1.52$ eV was obtained, indicating that another process limits the electrochemical performance in this range. This result, plus the fact that impedance diagrams are similar to those for LSM-YSZ or MIECs, strongly suggests the emergence of O^{2-} ion diffusion as an important mechanism in nanostructured LSM at low temperature. A similar "two-regime" behavior was also observed by Temperature Programmed Desorption and by Thermogravimetric Analysis (48) on ceramic nanostructured samples. Following those completely independent studies, the authors concluded that the electrochemical properties are dominated by diffusion at low temperature and by oxygen recombination (or charge transfer as described by Equation (3)) at high temperature, as we have obtained by direct measurements of the electrocatalytic properties of the nanostructured LSM cathodes. Therefore, ionic diffusion is likely to be the limiting process for temperatures below 800°C, while above this temperature, it is enhanced to the point of leaving a dominant charge transfer process.

Nanostructuring thus serves to overcome the limitation of gas phase transport of a porous LSM cathode and to increase its ionic conductivity, and both effects contribute to a qualitative enhancement in the global ORR process. Our results show that charge transfer dominates the cathodic properties at high temperatures. It is worth noting that dissociative adsorption should also be significant.

The evidences of ionic transport through the cathode (most likely through the surface of the cathode) can be understood within the following picture: As the rods are formed by nanoparticles, their surface disorder constitutes a proper environment for the presence of defects (such as oxygen vacancies) that gives rise to significant oxygen ion conduction. This is similar to Adler's idea for MIEC materials, according to which there is a penetration length that extends the reaction region for oxygen reduction beyond the TPB. In that picture MIEC conductivity arises from the interplay between this length and the size of the particles (49). Also, Hammouche et al. (50) ascribed the large electrocatalytic properties of LSM to the generation of oxygen vacancies that are mobile enough to carry oxygen from the electrode´s surface to the contact with the solid electrolyte. Thus, we think that surface disorder causes an extension of the ORR active region due to the formation of a high concentration of oxygen vacancies which in turn, gives rise to ionic conduction. The large surface-to-volume ratio in our cathode makes its contribution significant. In fact, in equivalent samples, a magnetic dead layer exists in the surface of the nanoparticles (50), which is related to a surface layer of a few nm of thickness and no long-range crystalline order that can be clearly distinguished from the core.

Moreover, evidences of ionic transport through dense LSM cathodes have also been shown in earlier studies (51,52). In addition, fast diffusion of oxygen at the grain boundaries has been observed by oxygen tracer experiments in A-site deficient La manganites (27) and in LSM (28), thus reinforcing our proposed picture.

Conclusions

Summarizing, we have studied the performance of nanostructured LSM cathodes, finding that their enhanced performance (in comparison to microstructured cathodes) is promising for their use IT-SOFCs. Qualitative changes have been obtained: cathodic properties are dominated by a charge transfer process and surface diffusion; not by gas phase transport. Those results are the consequence of the use of a porous nanostructure. The dominant process is consistent with the presence of significant ionic conductivity in nanostructured LSM.

Two operating regimes exist for the cathodic properties of nanostructured LSM cathodes: at high temperatures ionic conduction seems to limit the electrochemical behavior while for low temperatures, the limiting process is charge transfer.

The enhancement of ionic conductivity in nanostructured materials has been already observed in pure ionic conductors (15,16) and mixed electronic and ionic conductors (10,12) but, to the best of our knowledge, is the first time that it is found in a material with such low ionic conductivity as LSM. We consider that the surface disorder generated by the nanoparticles gives rise to oxygen vacancies which, in turn, contribute by increasing significantly ionic conductivity. In order to verify this hypothesis, we are presently studying the electrochemical properties of LSM cathodes exhibiting other nanostructures. Other cathode materials also deserve a similar study, since nanostructuration can give rise to enhanced performance.

Acknowledgements

Financial support from CONICET (PIP00038) and ANPCyT (PICT 1327, 1948 and 2689) is acknowledged. J.H.S. is currently at TENARIS, Siderca (Argentina). A.R.L. is currently at FCEN-UBA (Argentina). D.G.L. is currently at UNSAM (Argentina). We thank Paula Abdala for her assistance with samples preparation and EIS measurements and Solange Di Napoli and Cecilia Fischer for manuscript revision.

References

1. S. C. Singhal, K. Kendall, in *High-Temperature Solid Oxide Fuel Cells: Fundamentals, Design and Applications,* Elsevier, 2003.
2. Z. Shao, S. M. Haile. *Nature*, **431** (2004) 170-173.
3. Z. Jiang, C. Xia, F. Chen. *Electrochim. Acta*, **55** (2010) 3595‑3605.
4. V. Sadykov, V. Usoltsev, N. Yeremeev, N. Mezentseva, V. Pelipenko, T. Krieger, V. Belyaev, E. Sadovskaya, V. Muzykantov, Yu. Fedorova, A. Lukashevich, A. Ishchenko, A. Salanov, Yu. Okhlupin, N. Uvarov, O.

Smorygo, A. Arzhannikov, M. Korobeynikov, Ma.K.A. Thumm. *J. Eur. Ceram. Soc.*, **33** (2013) 2241-2250.
5. D. Han, H. Wu, J. Li, S. Wang, Z. Zhan. *J. Power Sources*, **246** (2014) 409-416.
6. J. Yoon, R. Araujo, N. Grunbaum, L. Baqué, A. Serquis, A. Caneiro, X. Zhang, H. Wang. *Appl. Surf. Sci*., **254** (2007) 266-269.
7. L. Baqué, A. Caneiro, M. S. Moreno, A. Serquis. *Electrochem. Comm*., **10** (2008) 1905-1908.
8. J. Yoon, S. Cho, J.-H. Kim, J.H. Lee, Zhenxing Bi, A. Serquis, X. Zhang, A. Manthiram and H. Wang. *Adv. Funct. Mater.*, **19** (2009) 3868–387.
9. M. G. Bellino, J. G. Sacanell, D. G. Lamas, A. G. Leyva and N. E. Walsöe de Reca. *J. Am. Chem. Soc*., **129** (2007) 3066–3067.
10. J. Sacanell, A. G. Leyva, M. Bellino, D. G. Lamas. *J. Power Sources*, **195** (2010) 1786-1792.
11. Li-Ping Sun, Qiang Li, Hui Zhao, Ju-Hong Hao, Li-Hua Huo, Guangsheng Pang, Zhan Shi, Shouhua Feng. *Int. J. Hydrogen Energy*, **37** (2012) 11955-11962.
12. L.M. Acuña, J. Peña-Martínez, D. Marrero-López, R.O. Fuentes, P. Nuñez, D.G. Lamas. *J. Power Sources*, **196** (2011) 9276-9283.
13. R. Pinedo, I. Ruiz de Larramendi, D. Jimenez de Aberasturi, I. Gil de Muro, J.I. Ruiz de Larramendi, M.I. Arriortua, T. Rojo. *J. Power Sources,* **196** (2011) 4174-4180.
14. I. Ruiz de Larramendi, R. Pinedo, N. Ortiz-Vitoriano, J.I. Ruiz de Larramendi, M.I. Arriortua, T. Rojo. *Physics Procedia*, **8** (2010) 2-9.
15. M. G. Bellino, D.G. Lamas, N.E. Walsöe de Reca. *Adv. Mater.,* **18** (2006) 3005–3009.
16. M. G. Bellino, D.G. Lamas, N.E. Walsöe de Reca. *Adv. Funct. Mater*., **16** (2006) 107–113.
17. Y. Ma, X. Wang, R. Raza, M. Muhammed, B. Zhu. *Int. J. Hydrogen Energy,* **35** (2010) 2580-2585.
18. P. M. Abdala, G. S. Custo, D. G. Lamas. *J. Power Sources,* **195** (2010) 3402-3406.
19. J. X. Wang, Y. K. Tao, J. Shao, W. Guo Wang., *J. Power Sources,* **186** (2009) 344-348.
20. Z. Wang, M. Cheng, Y. Dong, M. Zhang, H. Zhang. *Solid State Ionics,* **176** (2005) 2555.
21. T. Kenjo, M. Nishiya. *Solid State Ionics*, **57** (1992) 295.
22. J.H. Choi, J.H. Jang, J.H. Ryu, S.M. Oh. *J. Power Sources*, **87** (2000) 92-100.
23. S.P. Yoon, Jonghee Han, Suk Woo Nam, Tae-Hoon Lim, In-Hwan Oh, Seong-Ahn Hong, Young-Sung Yoo, Hee Chun Lim. *J. Power Sources,* **106** (2002) 160-166.
24. T. Suzuki, M. Awano, P. Jasinski, V. Petrovsky, H.U. Anderson. *Solid State Ionics*, **177** (2006) 2071-2074.
25. V.A.C. Haanappel, J. Mertens, D. Rutenbeck, C. Tropartz, W. Herzhof, D. Sebold, F. Tietz. *J. Power Sources,* **141** (2005) 216-226.
26. L. Hueso and N. Mathur, *Nature*, **427** (2004) 301-304.
27. A. V. Berenov, J. L. MacManus-Driscoll, J. A. Kilner. *Solid State Ionics*, **122** (1999) 41-49.
28. R. A. De Souza, J. A. Kilner, J. F. Walker. *Materials Lett*., **43** (2000) 43-52.

29. E. P. Murray, T. Tsai, S. A. Barnett. *Solid State Ionics*, **110** (1998) 235-243.
30. Thomsen, G.W. Coffey, L.R. Pederson, O.A. Marina, *J. Power Sources*, **191** (2009) 217-224.
31. Y. Takeda, R. Kanno, M. Noda, Y. Tomida, O. Yamamoto. *J. Electrochem. Soc.,* **134** (1987) 2656.
32. J. Im, I. Park and D. Shin, *Solid State Ionics,* **192** (2011) 448-452.
33. J.-D. Kim , G.-D. Kim, J.-W. Moon, Y.-i. Park, W.-H. Lee, K. Kobayashi, M. Nagai, C.-E. Kim. *Solid State Ionics*, **143** (2001) 379-389.
34. S. B. Adler, *Chem. Rev.*, **104** (2004) 4791-4843.
35. A. G. Leyva et al., *Journal of Solid State Chemistry*, **177** (2004) 3949–3953
36.
37. M. J. L. Ostergard, C. Clausen, C. Bagger, M. Mogensen. *Electrochim. Acta,* **40** (1995) 1971-1981.
38. E. Siebert, A. Hammouche, M. Kleitz. *Electrochim. Acta,* **40** (1995) 1741-1753.
39. B. C. H. Steele. *Solid State Ionics*, **94** (1997) 239-248.
40. M. Mamak, G. S. Métraux, S. Petrov, N. Coombs, G. A. Ozin , and M. A. Green. *J. Am. Chem. Soc*., **125** (2003) 5161-5175.
41. H. Kamata, A. Hosaka, J. Mizusaki, H. Tagawa. *Solid State Ionics*, **106** (1998) 237–245.
42. S.R. Gamble, J.T.S. Irvine. *Solid State Ionics*, **192** (2011) 394–397.
43. S. McIntosh, S. B. Adler, J. M. Vohs, R. J. Gorte. *Electrochem. Solid-State Lett.,* **7** (2004) A111-A114.
44. M. J. Jorgensen, M. Mogensen, *J. Electrochem Soc.,* **148** (2001) A433-A442.
45. E. Barsoukov, J. Ross Macdonald, *Impedance Spectroscopy: Theory, Experiment and Applications,* 2nd. edition*,* Wiley Interscience, New Jersey, 2005.
46. A. Ringuedé, J. Fouletier. *Solid State Ionics,* **139** (2001) 167-177.
47. O. J. Velle, T. Norby, P. Kofstad. *Solid State Ionics*, **47** (1991) 161-167.
48. N. Grunbaum, , L. Dessemond, J. Fouletier, F. Prado, L. Mogni, A. Caneiro. *Solid State Ionics*, **180** (2009) 1448-1452.
49. Rossetti, M. Allieta, C. Biffi, M. Scavini, *Phys. Chem. Chem. Phys*., **155** (2013) 16779-16787.
50. S. B. Adler, J. A. Lane and B. C. H. Steele. *J. Electrochem. Soc*., **143** (1996) 3554-3564.
51. A. Hammouche , E. Siebert, A. Hammou, M. Kleitz, and A. Caneiro. *J. Electrochem Soc*., **138** (1991) 1212.
52. J. Curiale, M. Granada, H. E. Troiani, R. D. Sánchez, A. G. Leyva, P. Levy, K. Samwer. *Appl. Phys. Lett*., **95** (2009) 043106.
53. J. Van Herle, A.J. McEvoy, K.Ravindranathan Thampi. *Electrochim Acta*, **41** (1996) 1447-1454.
54. T. Ioroi, T. Hara, Y. Uchimoto, Z. Ogumi, and Z. Takehara. *J. Electrochem. Soc.,* **144** (1997) 1362-1370.